Revista de Metalurgia 50(1)
January–March 2014, e001
ISSN-L: 0034-8570
doi: http://dx.doi.org/10.3989/revmetalm.001

Non-isothermal kinetics of the thermal desorption of mercury from a contaminated soil

Félix A. López[a,✉], María José Sierra[b], Olga Rodríguez[a], Rocío Millán[b], Francisco J. Alguacil[a]

[a]Centro Nacional de Investigaciones Metalúrgicas (CENIM), CSIC. Avda. Gregorio del Amo 8, 28040 Madrid, Spain
[b]Centro de Investigaciones Energéticas Medioambientales y Tecnológicas (CIEMAT) Avda. Complutense 22, 28230 Madrid, Spain
✉Corresponding author: flopez@cenim.csic.es

Submitted: 3 October 2013; Accepted: 11 November 2013

SUMMARY: The Almadén mining district (Ciudad Real, Spain) was the largest cinnabar (mercury sulphide) mine in the world. Its soils have high levels of mercury a consequence of its natural lithology, but often made much worse by its mining history. The present work examines the thermal desorption of two contaminated soils from the Almadén area under non-isothermal conditions in a N_2 atmosphere, using differential scanning calorimetry (DSC). DSC was performed at different heating rates between room temperature and 600 °C. Desorption temperatures for different mercury species were determined. The Friedman, Flynn-Wall-Ozawa and Coasts–Redfern methods were employed to determine the reaction kinetics from the DSC data. The activation energy and pre-exponential factor for mercury desorption were calculated.

KEYWORDS: Contaminated soils; DSC; Kinetic; Mercury; Thermal desorption

Citation / Cómo citar este artículo: López, F.A., Sierra, M.J., Rodríguez, O., Millán, R., Alguacil, F.J. (2014) “Non-isothermal kinetics of the thermal desorption of mercury from a contaminated soil”. *Rev. Metal.* 50(1): e001. doi: http://dx.doi.org/10.3989/revmetalm.001

RESUMEN: *Estudio cinético, en condiciones no-isotérmicas, de la desorción térmica del mercurio en suelos contaminados*. El distrito minero de Almadén (Ciudad Real, España) tiene la mayor mina de cinabrio (sulfuro de mercurio) del mundo. Sus suelos tienen altos niveles de mercurio como consecuencia de su litología natural, pero a menudo su contenido en mercurio es mucho más alto debido a la historia minera de la zona. Este trabajo examina la desorción térmica de dos suelos contaminados procedentes de Almadén bajo condiciones isotérmicas en atmósfera de N_2, empleando calorimetría diferencial de barrido (DSC). La calorimetría se llevó a cabo a diferentes velocidades de calentamiento desde temperatura ambiente hasta 600 °C. Se determinaron las diferentes temperaturas de desorción de las especies de mercurio presentes en los suelos. Para determinar la cinética de reacción a partir de los datos de DSC se utilizaron los métodos de Friedman, Flynn-Wall-Ozawa y Coasts–Redfern. Además se calcularon las energías de activación y los factores pre-exponenciales para la desorción del mercurio.

PALABRAS CLAVE: Cinética; Desorción térmica; DSC; Mercurio; Suelos contaminados

Copyright: © CSIC. This is an open-access article distributed under the terms of the Creative Commons Attribution-Non Commercial (by-nc) Spain 3.0 License.

1. INTRODUCTION

Mercury (Hg) is one of the most toxic of global pollutants (Gochfeld, 2003). Its toxicity depends on the type of exposure suffered and the chemical species involved being organic forms the most toxic (Luciana et al., 2012). Bioaccumulation and biomagnification intensify its ecological and toxicological impacts (Luciana et al., 2012 and Fitzgerald and Lamborg, 2003).

The mining districts of Almadén (Spain), Idrija (Slovenia) and Monte Amiata (Italy) have together produced more than half of the total Hg extracted and commercialized in the world. Although operations have now ceased, Almadén was the world's largest and oldest Hg mining operation, its production making up a full one third of the total Hg ever extracted (Hylander and Meili, 2003). This activity led to the gradual dissemination and redistribution of Hg in the surrounding area. Millán et al., (2006) and Millán et al., (2011) report Hg to be present in concentrations of up to 40,000 mg kg^{-1} in the soils affected by mining activities. Even areas further away from the centres of exploitation were affected by the atmospheric and hydrological transport of Hg (Higueras et al., 2003).

In others countries, small-scale gold (Au) mining activities are harmful to the environment in part because of the widespread use of Hg in the extraction process. After thoroughly grinding Au-containing ore or silt, Hg is added, creating an amalgam. Subsequent heating concentrates the gold into a pellet but releases elemental mercury into the environment (Paruchuri et al., 2010). In soil samples collected from the Tapajós (Brazil) gold mining reserve, the total mercury concentration in soil is nearly 13 times that recorded for background sites (Egler et al., 2006).

The technologies used to remove or stabilize Hg in contaminated solid waste or soil include solidification/stabilization, soil washing, thermal treatment, solar thermal desorption, vitrification and electrokinetic remediation. A comparison of the different technologies is provided by Wang et al. (2012) and López-Delgado et al. (2012a and 2012b) the Resource Conservation and Recovery Act (RCRA) of the United States suggests that Hg-containing waste be treated by solidification/stabilization when the Hg content is less than 260 mg kg^{-1}, and that thermal desorption methods be used when the Hg values are higher than 260 mg kg^{-1} (USEPA, 2008).

Thermal desorption treatment usually involves an *ex situ* technology that converts mercurial compounds into volatile Hg. The safety and reduced emissions due to the use of suitable filters associated with these techniques have led to their becoming preferred technologies in this field (Chang and Yen, 2006). Hg thermal desorption experiments have demonstrated the feasibility of mercury removal at temperatures between 127 °C and 600 °C (Kunkel et al., 2006).

Table 1. Desorption temperatures of different mercury phases in contaminated soils (Kunkel et al., 2006 and Biester et al., 2000)

Phase	Desorption temperature of phase Hg (°C)
Hg^0	<100
Non Cinnabar Hg	150–250
Hg_2Cl_2	<180
$HgCl_2$	<250
HgS (Cinnabar)	310–350
HgO	420–550
$HgSO_4$	450–500
Hg in Pyrite	>450
Hg in Sphalerite	600

Thermal decomposition techniques have been used to identify Hg compounds in soil, sediment samples, iron-based sorbents, and even in Hg lamp waste. The Hg species thermally released from contaminated soils can be analysed in several ways, including temperature-controlled continuous heating of samples in a furnace coupled to an atomic absorption spectrophotometer (AAS) (Windmoller et al., 1996) the use of solid-phase Hg-thermodesorption techniques complemented by selective extraction of organically bound Hg (Biester et al., 2000) by temperature programmed decomposition desorption (TPDD) (Ozaki et al., 2008), or by pyrolysis and X-ray absorption fine spectroscopy (XAFS) (Liu et al., 2006). Table 1 shows the mercury speciation derivatives recorded by different researchers.

In the present work, the thermal desorption of Hg was analyzed by differential scanning calorimetry (DSC) in a N_2 atmosphere, with the aim of elucidating the associated reaction mechanisms and kinetics.

2. MATERIALS AND METHODS

2.1. Samples

The material analysed consisted of two Hg-contaminated soils (S1 and S2) from the Almadén area (Fig. 1). Soil S1 (34 mg kg^{-1} of total Hg) was taken from Dehesa de Castilseras (northeast of the El Entredicho mine). The area is an open Mediterranean forest where livestock graze. The Hg concentration of this soil is lower than the other soil S2 (Table 2) and is mainly of natural origin although this site has also been affected by mining activity. Soil S2 (10,497 mg kg^{-1} of total Hg) was from an abandoned metallurgical site in Almadenejos. This site dates from the 18th century and lies 12 km from

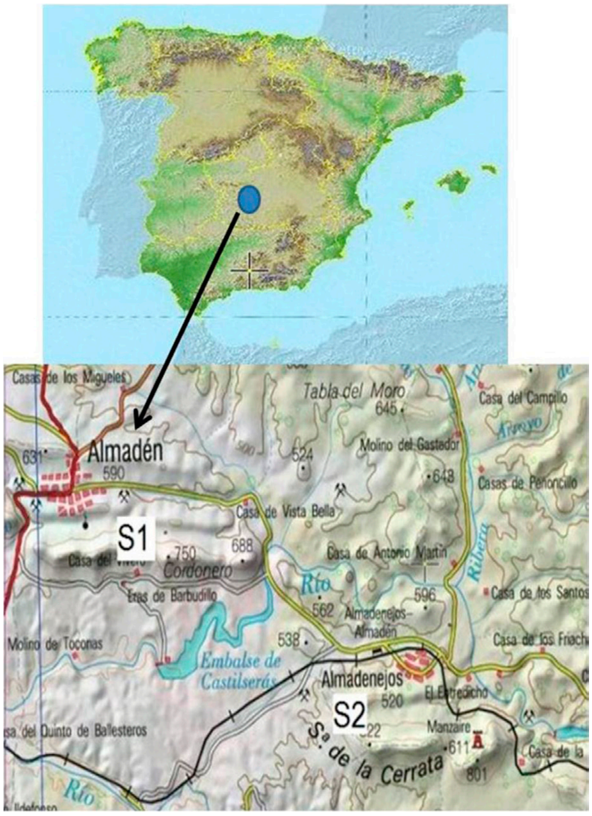

Figure 1. Location of soil collection sites.

Almadén. It occupies an area of some 30,000 m^2 and is surrounded by a wall built between 1756 and 1759. The area contains six pairs of abandoned roasting furnaces once used to obtain primary Hg from cinnabar. The soil in this area has a high Hg concentration (Table 2) - partly of natural origin and partly the result of mining activity, Hg waste storage, and the use of these cinnabar roasting furnaces (Millán et al., 2011). As sampling strategy, a composite sample of each study soil was collected from a 5 m^2 by obtaining 10 cm of the surface soil at five points. Afterwards, both soil samples were air dried and sieved to obtain the fraction less than 2 mm ready for the different analysis and trials.

Furthermore, reference materials with known concentrations of Hg were used: CRM 051 from an Hg-contaminated area (29.9±5.96 mg kg^{-1} of total Hg) in the western USA, and SRM 2709a, an agricultural soil (1.40±0.08 mg kg^{-1} of total Hg) from San Joaquín (Querétaro, Mexico).

2.2. Physico-chemical analysis of soils

The pH (H_2O, 1:2.5) and electrical conductivity (EC) (H_2O, 1:5) of the soils were measured according to the official methods of the Spanish Ministry of Agriculture, Fisheries and Food (MAPA, 1994). The EC of the saturated extract $(EC)_{ES}$ was determined by multiplying EC by 6.4 according to the method proposed by Loveday et al., (1972). The organic matter (OM) content of the soils was determined using the method of Walkley-Black and the soil textures recorded using the Bouyoucos method, according to standard procedures (Page et al., 1987).

2.3. Determination of soil Hg concentration

The Hg concentration of the soil samples was directly measured using an atomic absorption spectrophotometer specifically designed for Hg determination (Advanced Mercury Analyser - AMA254 – LECO Company). The certified reference material CRM 051 (soil from USA contaminated area, 29.90±5.96 mg kg^{-1} of total Hg) was used as a standard to determine the accuracy and precision of the measurements and to validate the applied method. The mean value of total Hg determined for 10 measurements of the certified material using the AMA254 equipment was 29.90±2.89 mg kg^{-1} of total Hg. At a 95% confidence level, no significant differences were detected between the certified value and the experimental one, this method was therefore considered to be reliable for the determination of total Hg.

When samples showed a high Hg content, out of equipment range limit (>600 ng), they were preprocessed by an acidic digestion using a MARS5 microwave oven (VERTEX Technics) following EPA Method 3052 (USEPA, 1996) in order to dilute for measuring by the above analyser. Recovery percentage for certified reference material (CRM 051) was 99%.

Table 2 shows the physico-chemical characteristics of the contaminated and reference soils.

Table 2. Physico-chemical characteristics of contaminated soils

Soil	pH	EC (1:5) (µS cm^{-1})	EC_{ES} (dS cm^{-1})	Organic Matter (wt. %)	Texture	Hg (mg kg^{-1})
S1	6.9	164	1.05	2.8	Sandy loam	34.40±7.20
S2	6.1	614	3.93	3.7	Sandy loam	10,497±1,564
SRM 2709a	–	–	–	–	–	1.40±0.08
CRM 051	–	–	–	–	–	29.90±5.96

2.4. Thermal desorption study soil constituents

S1, S2, CRM 051 and SRM 2709a were subjected to DSC analysis in a N_2 atmosphere (flow rate 20 mL min^{-1}). About 60 mg of each sample were placed in a 175 μL sealed aluminium crucible and heated at a rate of 10 °C min^{-1} between 25 and 600 °C or 650 °C in a Setaram Model 3D-EVO analyser, which also recorded the temperature peaks associated with Hg desorption.

2.5. Differential scanning calorimetry kinetics: Mathematical models for determining Hg desorption kinetics

The kinetics of Hg desorption were then studied by DSC using the apparatus mentioned above. DSC experiments were performed at four different heating rates (5, 10, 15, and 20 °C min^{-1}) between room temperature and 600 °C. Temperature calibration was achieved using ICTAC-recommended DSC standards. The accuracy of the reported temperatures was estimated to be ±2 °C. The sample mass used was again about 60 mg, and all experiments were performed in a N_2 atmosphere (flow rate 20 mL min^{-1}).

For mercury desorption, it is generally assumed that the rate of conversion is proportional to the concentration of reacted material. The rate of conversion can be expressed by the following basic rate equation (Eq. 1):

$$\frac{d\alpha}{dt} = \beta\frac{d\alpha}{dT} = k(T).f(\alpha) \tag{1}$$

where α is the degree of advance of reaction, $f(\alpha)$, β the heating rate (°C min^{-1}) and $k(T)$ are functions of conversion and temperature. For the DSC experiments, equation (2) can be expressed as:

$$\frac{d\alpha}{dt} = \frac{dH}{dt}.\frac{1}{\Delta Htotal} \tag{2}$$

where $\frac{dH}{dt}$ is the heat flow above baseline and $\Delta Htotal$ the peak area of the reaction, expressed in mJ.

By combining equations (1) and (2), the rate of conversion can be written in the form Eq. (3):

$$\frac{d\alpha}{dt} = \frac{dH}{dt}.\frac{1}{\Delta Htotal} = k(T).f(\alpha) \tag{3}$$

where $k(T)$ is the temperature dependent on the rate of heat flow; this is often modelled successfully by the Arrhenius Eq. (4):

$$k(T) = Ae^{-E/RT} \tag{4}$$

where E (kJ/mol) is the activation energy, A (min^{-1}) the pre-exponential factor, and R (8.314 J mol^{-1} K^{-1}) the gas constant. By combining equations (3) and (4), the reaction rate can be written as Eq. (5):

$$\frac{d\alpha}{dt} = Ae^{-E/RT}f(\alpha) \tag{5}$$

Friedman method

Friedman analysis (Friedman, 1964), which is based on the Arrhenius equation (4), takes into account the logarithm of the conversion rate ($d\alpha/dt$) as a function of the reciprocal of the temperature (i.e., $1/T$) at different degrees of conversion α, according to Eq. (6):

$$\ln\frac{d\alpha}{dt}|_{\alpha i} = \ln(A_i f(\alpha_{i,j})) - \frac{E_{ai}}{R.T_{i,j}} \tag{6}$$

where i is the index of conversion, j is the curve index, E_a the apparent activation energy at α_i, and $f(\alpha_{i,j})$ the function dependent on the reaction model (assumed to be constant for a given reaction progress $\alpha_{i,j}$ for all curves j). Since $f(\alpha)$ is constant at each degree of conversion αi, the curve for the logarithm of the reaction rate vs. $1/T$ is linear, with a slope of E_a/R and an intercept A.

Flynn-Wall-Ozawa method

The Flynn-Wall-Ozawa method (Flynn and Wall, 1996 and Ozawa, 1965) is derived from the integral isoconversional method. Using Doyle's approximation (Doyle, 1961) the reaction rate in logarithmic form can be expressed as Eq. (7):

$$\ln\beta = \ln\left(\frac{AE_a}{R\cdot g(\alpha)}\right) - 5.331 - 1.052\frac{E_a}{R}\frac{1}{T} \tag{7}$$

where β is the heating rate and $g(\alpha)$ is the function of conversion. Thus, for any constant α value, the plot ln β vs. $1/T$ recorded at different heating rates should be a straight line. The E_a can be then determined from its slope.

Coats-Redfern method

The Coats-Redfern method (Coats and Redfern, 1964) provides the thermal decomposition mechanism from the mass loss. An asymptotic approximation of $2RT/E_a<1$ for the resolution of Eq. (8):

$$g(\alpha) = \int_0^\alpha \frac{d\alpha}{f(\alpha)} = \frac{A}{\beta}\int_{T_0}^{T}\exp\left(\frac{E_a}{RT}\right)dT$$
$$= \frac{AE_a}{\beta R}p\left(\frac{E_a}{RT}\right) \tag{8}$$

TABLE 3. Algebraic expressions of functions of the most common reaction mechanisms

Mechanism	$f(\alpha)$	$g(\alpha)$
Autocatalytic	$(1-\alpha)^n.\ \alpha^m$	–
Avarani-Erofe've (A1.5)	$1.5(1-\alpha)\ [-\ln(1-\alpha)]^{1/3}$	$[-\ln(1-\alpha)]^{1/3}$
Avarani-Erofe've (A2)	$2(1-\alpha)\ [-\ln(1-\alpha)]^{1/2}$	$[-\ln(1-\alpha)]^{1/2}$
Avarani-Erofe've (An)	$n(1-\alpha)\ [-\ln(1-\alpha)]^{(1-1/n)}$	$[-\ln(1-\alpha)]^{(1-1/n)}$
First-order (F1)	$(1-\alpha)$	$-\ln(1-\alpha)$
Second-order (F2)	$(1-\alpha)^2$	$(1-\alpha)^{-1}-1$
Third-order (F3)	$(1-\alpha)^3$	$[(1-\alpha)^{-2}-1]/2$
Contracting sphere (R2)	$2(1-\alpha)^{1/2}$	$[1-(1-\alpha)^{1/2}]$
Contracting Cylinder (R3)	$3(1-\alpha)^{2/3}$	$[1-(1-\alpha)^{1/3}]$
Power law (P2)	$2\alpha^{1/2}$	$\alpha^{1/2}$
Power law (P3)	$3\alpha^{2/3}$	$\alpha^{1/3}$
Power law (P4)	$4\alpha^{3/4}$	$\alpha^{1/4}$
One-dimensional diffusion (D1)	$1/2\alpha$	α^2
Two-dimensional diffusion (D2)	$[-\ln(1-\alpha)]^{-1}$	$[(1-\alpha)\ln(1-\alpha)]+\alpha$
Three-dimensional diffusion (D3)	$3(1-\alpha)^{(2/3)}]/[2(1-(1-\alpha)^{(1/3)})]$	$[1-(1-\alpha)^{1/3}]^2$
Giustling-Brounsthein (D4)	$1.5\ ((1-\alpha)^{(-1/3)}-1)$	$1-(2\alpha/3)-(1-\alpha)^{2/3}$

allows equation (9) to be obtained:

$$\ln\frac{g(\alpha)}{T^2}=\ln\frac{AR}{\beta E}-\frac{E_a}{RT} \tag{9}$$

The Coats-Redfern method is one of the most widely used procedures for the determination of reaction processes. The E_a at a constant heating rate for any of the $g(\alpha)$ functions listed in Table 3 can be obtained from equation (9).

3. RESULTS

3.1. Thermal decomposition of contaminated and reference soils

Figure 2 shows the DSC curves by heating the soils at a rate of 10 °C min^{-1} from room temperature to 650 °C. Two or three endothermic peaks can be seen. Table 4 shows the temperature data for these peaks.

Three peaks can be seen for S1, with maximum temperatures (T_m) of 109.5 °C, 304.8 °C and 533.8 °C. S2 has only two peaks of T_m 121.8 °C and 305.7 °C.

CRM 051 has two peaks of T_m 93.4 °C and 546.4 °C, while SRM 2079a has three of T_m 122.5 °C, 279.2 °C and 528.5 °C.

Using the data in Table 1 as a reference, Hg is released from $HgCl_2$ between 72 and 182 °C, according to the reaction $HgCl_2\,(s) \rightarrow Hg(g) + 2Cl(g)$ (peak 1 in the DSC curves; see Fig. 2). In a well-aerated soil as is the case of the study soils, the conditions are normally appropriate for the formation of inorganic Hg^{2+} as $HgCl_2$. The mercurous cation is rarely stable under ambient conditions and, together with Hg^0 is easily oxidized to Hg^{2+}. Therefore, Hg form mainly present in the soil will be $HgCl_2$ (Adriano, 2001 and Gaona, 2004).

The peak of T_m=93.4 °C in the DSC curve for CRM 051 could be due to the desorption of

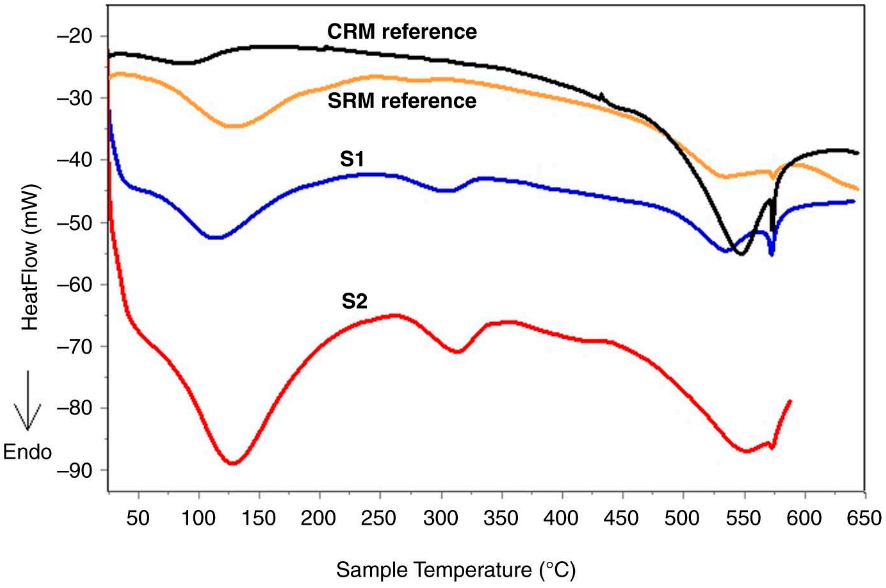

FIGURE 2. DSC curves of thermal decomposition of contaminated soils and references (Heating rate: 10 °C min^{-1}).

Table 4. DSC results for the thermal desorption of Hg from the contaminated and references soils (heating rate: 10 °C min^{-1})

	Peak 1			Peak 2			Peak 3		
Soil	**T_o (°C)**	**T_m (°C)**	**T_e (°C)**	**T_o (°C)**	**T_m (°C)**	**T_e (°C)**	**T_o (°C)**	**T_m (°C)**	**T_e (°C)**
S1	74.3	109.5	141.3	266.7	304.8	327.2	506.4	533.8	554.8
S2	72.3	121.8	182.1	269.0	305.7	330.0	–	–	–
SRM	78.0	122.5	172.5	265.3	279.2	296.2	505.6	528.5	559.5
CRM	50.6	93.4	127.8	–	–	–	512.8	546.4	564.5

(T_o: Start of peak temperature; T_m: maximun temperature; T_e: End of peak temperature)

metallic Hg (Hg^0), according to the reaction $Hg^0(s) \rightarrow Hg(g)$. This peak is not seen in any other DSC curve.

The decomposition of cinnabar (HgS) occurs between 267 and 327 °C, according to the reaction $HgS(s) \rightarrow Hg(g) + S(g)$ (peak 2 in the DSC curves; see Fig. 2).

Finally, HgO decomposes at 505–565 °C according to the reaction $HgO(s) \rightarrow Hg(g) + \frac{1}{2} O_2(g)$ (peak 3 in the DSC curves; see Fig. 2).

The T_m values for desorption of Hg from the different phases of the contaminated soils follow the order $Hg^0 < HgCl_2 < HgS < HgO$. These temperatures agree quite well with those reported by other authors using other techniques (Windmoller, 1996 and López et al., 2010). This order suggests that the thermal release of mercury species is related to its vapour pressure (Stein et al., 1996). When the vapour pressure decreases, the Hg release temperature increases.

Hg is subject to a wide array of chemical and biological transformation processes, such as Hg^0 oxidation, Hg^{2+} reduction, and methylation, depending on the soil pH, temperature, and humus content. The formation of organic Hg^{2+} complexes is known to be a dominant process, largely due to the affinity of Hg^{2+} and its inorganic compounds for sulphur-containing functional groups (Skyllberg et al., 2006).

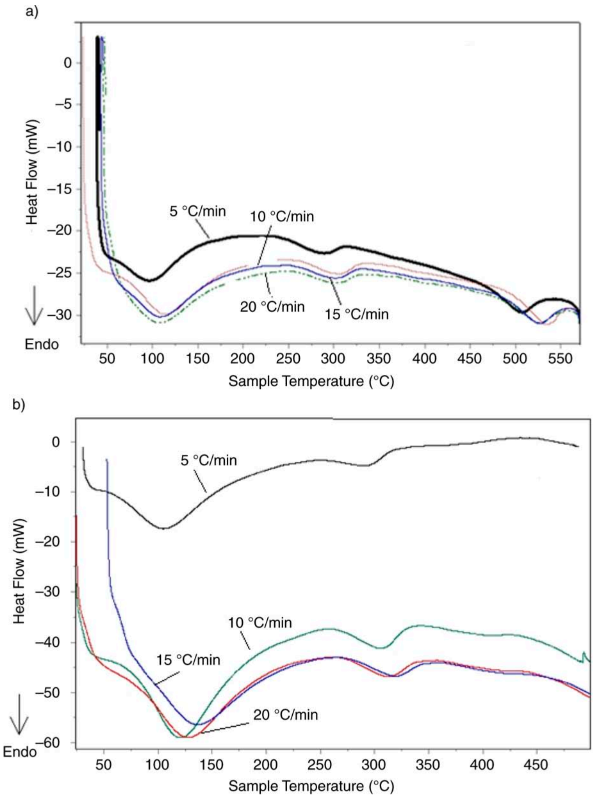

Figure 3. DSC curves for the decomposition of contaminated soils at different heating rates. a) for S1 and b) for S2.

Table 5. DSC data for the thermal decomposition of the soils at different heating rates

	Peak 1			Peak 2			Peak 3		
β (°C min^{-1})	**T_o (°C)**	**T_m (°C)**	**T_e(°C)**	**T_o (°C)**	**T_m(°C)**	**T_e (°C)**	**T_o (°C)**	**T_m (°C)**	**T_e (°C)**
S1									
5	60.8	95.1	122.7	251.6	284.9	309.0	493.1	507.6	524.2
10	74.3	109.5	142.3	266.7	304.8	327.2	495.0	526.0	549.7
15	74.9	110.9	149.7	261.7	300.9	325.8	566.9	572.3	575.9
20	73.5	108.6	151.6	262.6	301.0	324.6	564.2	572.1	577.9
S2									
5	61.5	103.6	141.5	260.6	294.1	314.3	–	–	–
10	72.3	121.8	146.7	269.0	305.7	330.0	–	–	–
15	85.7	122.5	149.4	274.8	312.3	335.9	–	–	–
20	96.9	129.8	154.3	279.2	318.2	343.0	–	–	–

Table 6. Activation energies for S1 and S2, as determined by the Friedman and the Flynn-Wall-Ozawa methods

		FR method		FWO method
Peak / Reaction	**Soil**	**Ea (kJ mol^{-1})**	**A (s^{-1})**	**Ea (kJ mol^{-1})**
Peak 1:	S1	44.6±3.9	7.74×10^{3}	53.0±4.8
$HgCl_2 \rightarrow Hg (g) + 2Cl (g)$	S2	49.7±3.0	1.54×10^{4}	55.7±3.3
Peak 2:	S1	138.6±	4.73×10^{10}	145.0±7.6
$HgS \rightarrow Hg (g) + S (g)$	S2	188.7±9.8	1.01×10^{15}	186.7±12.3
Peak 3:	S1	255.2±	5.95×10^{14}	284.4±2.7
$HgO \rightarrow Hg (g) + \frac{1}{2} O_2 (g)$	S2	–	–	–

Besides the above mentioned peaks, all samples show a sharp endothermic peak at 575 °C, that could be attributed to the polymorphic transformation of hypothermic quartz to hyperthermic quartz which starts at this temperature. It is due to the phase transition in quartz (α-Quartz trigonal to β-Quartz hexagonal) (Karathanasis et al., 1994; Plante et al., 2009; Salgado et al., 1995 and Salgado et al., 2004). X-ray diffraction of soil samples shows that the percentage of quartz in soil S1 (82%) is higher than the soil S2 (60%). This result is in agreement with the different depth of the S1 and S2 peaks. Thereby, the peak of S1 is deeper than the peak of S2.

Figure 3 show the DSC curves for S1 and S2 at different heating rates (5, 10, 15 and 20 K min^{-1}). Table 5 shows the T_m values for the peaks obtained. A shift towards higher T_m values was seen as the heating rate increased (Fig. 3). This displacement of DSC curves with heating rate has been described by other researchers (Aboulkas et al., 2010).

Both soils present the same two firs peaks showing similar chemical bonds. However soil S1 has a third peak which does not appear in the case of S2. Therefore, S1 seems to have significantly more HgO than S2 has.

3.2. Calculation of the activation energy

The Friedman (FR) and the Flynn-Wall-Ozawa (FWO) methods were first used to calculate the E_a for all heating rates.

With the FR method, the E_a was calculated for different conversion values by plotting $\ln(d\alpha/dT)$ against $1/T$ for a constant α value. Table 6 shows the results for S1 and S2.

Equation (7) was used with the FWO method. The results supplied are independent of the degradation mechanism. The E_a for S1 and S2 were obtained from the plot of log (β) vs. $1/T$ at a fixed conversion rate (the slope being 0.4567E/R). Table 6 shows the E_a values for S1 and S2.

The E_a values obtained with the FWO method were higher than those obtained by the FR method. This is to be expected since the FWO method involves a systematic error that does not affect the FR method (Vyazovkin, 2001). The E_a values obtained by the FR method are therefore deemed more reliable.

For all the decomposition reactions studied, the variation in E_a with the degree of conversion over the interval 0.1<α<0.9 was practically constant (Figure 4). This suggests that these Hg reactions occur in a single stage.

The variation in E_a, independent of the calculation method used, shows that E_a $HgCl_2$<E_a HgS<E_a HgO. The vapour pressure and decomposition T_m values for each Hg compound follow the same order.

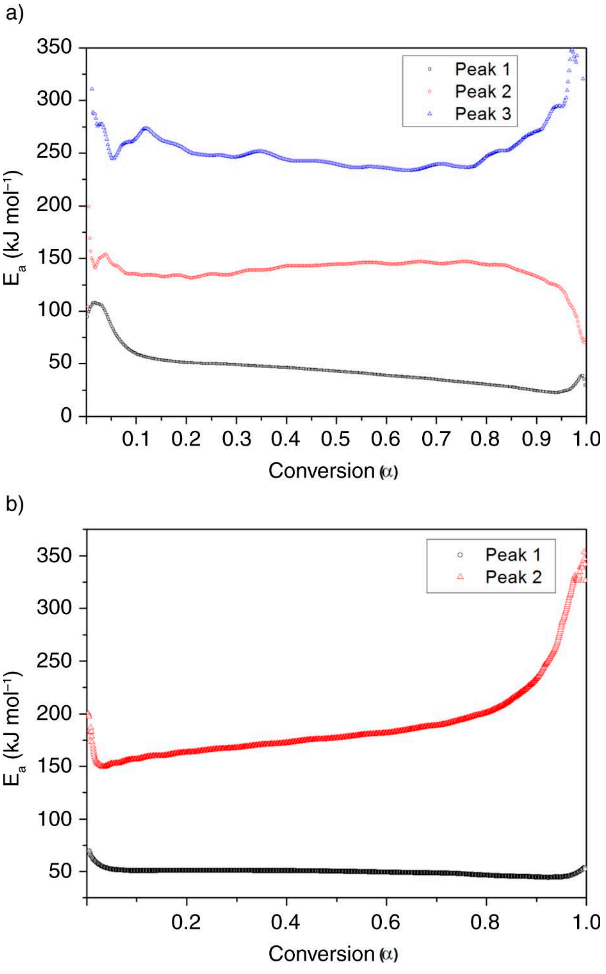

Figure 4. Apparent activation energy, as determined by the Friedman method for a) Soil S1 and b) Soil S2.

Table 7. Activation energies and pre-exponential factors for S1 and S2 as determined by the Coasts-Redfern method for different *f(α)* functions

	S1						S2			
	$HgCl_2 \rightarrow Hg(g)+2Cl(g)$		$HgS \rightarrow Hg(g)+S$		$HgO \rightarrow Hg(g)+½O_2\ (g)$		$HgCl_2 \rightarrow Hg(g)+2Cl(g)$		$HgS \rightarrow Hg(g)+S$	
Model	E_a (kJ mol^{-1})	A (s^{-1})	E_a (kJ mol^{-1})	A (s^{-1})	E_a (kJ mol^{-1})	A (s^{-1})	E_a (kJ mol^{-1})	A (s^{-1})	E_a (kJ mol^{-1})	A (s^{-1})
Autocatalytic	33.92	2.56×10^{2}	137.05	3.45×10^{10}	4.44×10^{-5}	1.46×10^{-2}	47.34	1.15×10^{-4}	176.46	1.06×10^{14}
A1.5	14.99	3.2×10^{-1}	103.97	2.31×10^{7}	231.26	1.25×10^{13}	24.42	5.92	123.86	1.2×10^{9}
A2	7.02	2.17×10^{-2}	75.74	4.57×10^{4}	170.35	9.61×10^{8}	15.78	3.6×10^{-1}	95.07	2.37×10^{6}
An	21.34	2.57	139.58	5.45×10^{10}	4.64×10^{-5}	2.61×10^{3}	39.51	6.76×10^{2}	173.84	5.19×10^{13}
F1	30.93	5.73×10^{2}	160.52	4.99×10^{12}	353.07	1.8×10^{21}	41.69	1.33×10^{3}	181.45	2.61×10^{14}
F2	66.43	1.02×10^{7}	272.63	3.54×10^{23}	601.04	1.27×10^{28}	78.90	2.68×10^{8}	295.76	1.82×10^{25}
F3	101.93	1.82×10^{12}	384.83	2.51×10^{34}	849	8.92×10^{54}	116.10	5.17×10^{13}	410.08	1.26×10^{36}
Fn	44.43	5.69×10^{3}	151.39	6.67×10^{11}	359.16	4.66×10^{21}	53.22	5.8×10^{4}	187.76	1.04×10^{15}
R2	13.18	6.79×10^{-2}	104.32	9.36×10^{6}	229.09	3.39×10^{12}	23.09	1.49	124.29	4.94×10^{8}
R3	19.09	3.4×10^{-1}	123.02	4.02×10^{8}	270.42	1.45×10^{15}	29.29	7.6	143.34	2.11×10^{10}
Rn	44.43	-2.16×10^{3}	151.39	5.37×10^{10}	359.16	-1.14×10^{20}	53.22	-1.8×10^{4}	187.76	-5.73×10^{13}
P2	−21.76	1.23×10^{-6}	−14.75	8.24×10^{-5}	–	2.4×10^{-5}	−14.34	1.92×10^{-5}	2.83	4.29×10^{-3}
P3	−27.49	1.62×10^{-7}	−35.74	7.3×10^{-7}	−74.99	1.98×10^{-8}	−20.62	2.28×10^{-6}	−18.61	3.77×10^{-5}
P4	−30.357	5.38×10^{-8}	−46.24	6.31×10^{-8}	−97.51	5.21×10^{-10}	−23.75	7.23×10^{-7}	−29.33	3.25×10^{-6}
D1	29.80	1.1×10^{1}	174.15	2.56×10^{13}	375.26	1.44×10^{22}	42.15	4.15×10^{2}	195.75	1.43×10^{15}
D2	43.24	5.59×10^{2}	217.57	2.1×10^{17}	470.55	2.24×10^{28}	56.31	2.25×10^{4}	239.89	1.14×10^{19}
D3	61.52	6.23×10^{4}	275.20	1.74×10^{22}	598	2.26×10^{36}	75.45	2.63×10^{6}	298.62	9.35×10^{23}
D4	49.68	1.11×10^{3}	237.80	4.19×10^{18}	515.35	5.47×10^{30}	63.05	4.52×10^{4}	260.51	2.27×10^{20}

The E_a of each reaction was greater for S2 than for S1, in agreement with the quantity of Hg in each soil.

Employing equation (9), the Coast-Redfern method was also used to determine the E_a values for all the *f(α)* functions listed in Table 2 at a constant heating rate. Table 7 shows the E_a and *A* values for S1 and S2 at a constant heating rate of 10 °C min^{-1}.

Table 8 summarises E_a and *A* values and the thermal degradation mechanisms determined by the Coats-Redfern method. The thermal desorption of $HgCl_2$ is likely to be of the F_n type since this mechanism has an E_a (44.4 kJ mol^{-1} for S1 and 53.2 kJ mol^{-1} for S2), similar to that obtained by the FR method (44.6 kJ mol^{-1} for S1 and 49.7 kJ mol^{-1} for S2). The thermal degradation mechanism of HgS is probably A_n-type (n=1.1) for S1 and F_n (n=1.06) for S2. The thermal degradation mechanism of $HgCl_2$ is F_n-type (n=1.38 for S1 and n=1.31 for S2). Finally, the thermal degradation mechanism of HgO is likely A_n-type (n=1.5).

L'vov (1999) reported an E_a for the decomposition of pure HgO of 201.7±3 kJ mol^{-1} in an O_2 atmosphere, and of 93±8 kJ mol^{-1} in a vacuum. Later, L'vov et al. (2004) reported a value of 186±1 kJ mol^{-1} in O_2. The literature appears to have no information on the decomposition energies of $HgCl_2$ and HgS.

4. CONCLUSIONS

The E_a was found to be practically constant over the 0.1–0.9 α interval for S1 and S2, suggesting that the decomposition of Hg compounds

Table 8. Activation energies of S1 and S2 as obtained by the Coats-Redfern method

Peak/Reaction		E_a (kJ mol^{-1})	A (s^{-1})	**Thermal decomposition mechanism**
Peak 1: $HgCl_2 \rightarrow Hg\ (g)+2Cl\ (g)$	S1	44.4	5.69×10^{3}	Fn: $(1-\alpha)^{1.38}$ (n=1.38)
	S2	53.2	5.80×10^{4}	Fn: $(1-\alpha)^{1.31}$ (n=1.31)
Peak 2: $HgS \rightarrow Hg\ (g)+S\ (g)$	S1	139.6	5.45×10^{10}	$A_n=n(1-\alpha)[-\ln(1-\alpha)^{(1-1/n)}$ (n=1.1)
	S2	187.8	1.04×10^{15}	Fn: $(1-\alpha)^{n}$ (n=1.06)
Peak 3: $HgO \rightarrow Hg\ (g)+½\ O_2\ (g)$	S1	231.3	1.25×10^{13}	$A_n=n(1-\alpha)[-\ln(1-\alpha)^{(1-1/n)}$ (n=1.5)
	S2	–	–	–

is a single-step process with an E_a of 44–53.2 kJ mol^{-1} for $HgCl_2$, 139.6–187.8 kJ mol^{-1} for HgS, and 231 kJ mol^{-1} for HgO. The corresponding E_a and A values were calculated in order to interpret the relationships between the soils. The Coats–Redfern method was successfully used to predict the reaction mechanism of thermal degradation of Hg compounds. The decomposition reaction model for $HgCl_2$ is first order, whereas that of HgO is described by the Avarani-Erofe've model, and that of HgS is first order and also described by the Avarani-Erofe've model, depending on the soil type. Knowledge of these E_a values could be important when attempts are made to remediate Hg-contaminated soils by thermal decomposition.

ACKNOWLEDGMENTS

This work was funded by MAYASA and the Centro Tecnológico Nacional para la Descontaminación del Mercurio (CTNDM).

Dr. O. Rodríguez is the recipient of contract JAE-Doc_09-00121 (CSIC), co-funded under the FSE 2007-2013 Multiregional Adaptability and Employment Operational Programme.

NOMENCLATURE

DSC: Differential Scanning Calorimetry
E: Activation energy (kJ mol^{-1})
dH/dt: Heat flow (mW)
E_a: Apparent activation energy at α (kJ mol^{-1})
A: Pre-exponential factor (s^{-1})
α: conversion
n and m: reaction order
R: gas constant (J mol^{-1} K^{-1})
T: Temperature (°C)
T_m: Maximum temperature peak (°C)
β: Heating rate (°C min^{-1})
$f(\alpha)$: Functions of conversion
$g(\alpha)$: Integral function of conversion

REFERENCES

Aboulkas, A., El Harfi, K., El Bouadili, A. 2010. Thermal degradation behaviors of polyethylene and polypropylene. Part I: Pyrolysis kinetics and mechanisms. *Energ. Convers. Manage.* 51 (7), 1363–1369. http://dx.doi.org/10.1016/j.enconman.2009.12.017.

Adriano, D.C. 2001. Chapter 11. Mercury. Trace Elements in the Terrestrial Environments. 2nd Edition ed. New York: Springer; 2001. pp. 411–458.

Biester, H., Gosar, M., Covelli, S. 2000. Mercury speciation in sediments affected by dumped mining residues in the drainage area of the Idrija mercury mine, Slovenia. *Environ. Sci. Technol.* 34 (16), 3330–3336. http://dx.doi.org/10.1021/es991334v.

Coats, A.W., Redfern, J.P. 1964. Kinetic parameters from thermogravimetric data. *Nature* 201 (491), 68–70. http://dx.doi.org/10.1038/201068a0.

Chang, T.C., Yen, J.H. 2006. On-site mercury-contaminated soilsremediation by using thermal desorption technology. *J. Hazard. Mater.* 128 (2–3), 208–217. http://dx.doi.org/10.1016/j.jhazmat.2005.07.053.

Doyle, C.D. 1961. Kinetic analysis of thermogravimetric data. *J. Appl. Polym. Sci.* 5 (15), 285–292. http://dx.doi.org/10.1002/app.1961.070051506.

Egler, S.G., Rodrigues, S., Villas-Boas, R.C., Beinhoff, C. 2006. Evaluation of mercury pollution in cultivated and wild plants from two small communities of the Tapajo's gold mining reserve, Para State, Brazil. *Sci. Total. Environ.* 368 (1), 424–433. http://dx.doi.org/10.1016/j.scitotenv.2005.09.037.

Fitzgerald, W.F., Lamborg, C.H. 2003. Treatise on Geochemistry, Ed. Elsevier, Oxford (UK), pp. 107–148.

Flynn, J.H., Wall, L.A. (1966). A quick direct method for determination of activation energy from thermogravimetric data. *J. Polym. Sci. Pol. Lett.* 4 (5PB), 323–327. http://dx.doi.org/10.1002/pol.1966.110040504.

Friedman, H.L. 1964. Kinetics of thermal degradation of char-forming plastics from thermogravimetry. Applications to phenolic plastic. *J. Polym. Sci. Pol. Sym.* (6PC), 183–195.

Gaona Martínez, X. 2004. El mercurio como contaminante global. Desarrollo de metodologías para su determinación en suelos contaminados y estrategias para la reducción de su liberación al medio ambiente. Barcelona, Universidad Autónoma de Barcelona.

Gochfeld, M. 2003. Cases of mercury exposure, bioavailability, and absorption. *Ecotoxicol. Environ. Saf.* 56 (1), 174–179. http://dx.doi.org/10.1016/s0147-6513(03)00060-5.

Higueras, P., Oyarzun, R., Biester, H., Lillo, J., Lorenzo, S. 2003. A first insight into mercury distribution and speciation in soils from the Almaden mining district, Spain. *J. Geochem. Explor.* 80 (1), 95–104. http://dx.doi.org/10.1016/s0375-6742(03)00185-7.

Hylander, L.D., Meili, M. 2003. 500 years of mercury production: global annual inventory by region until 2000 and associated emissions. *Sci. Total. Environ.* 304 (1–3), 13–27. http://dx.doi.org/10.1016/s0048-9697(02)00553-3.

Karathanasis, A.D., Harris, W.G. 1994. Quantitative Methods in Soil Mineralogy, Ed. Soil Science Society of America, Madison WI, pp. 360–411.

Kunkel, A.M., Seibert, J.J., Elliott, L.J., Kelley, R., Katz, L.E., Pope, G.A. 2006. Remediation of elemental mercury using in situ thermal desorption (ISTD). *Environ. Sci. Technol.* 40 (7), 2384–2389. http://dx.doi.org/10.1021/es0503581.

L'Vov, B.V., Ugolkov, V.L., Grekov, F.F. 2004. Kinetics and mechanism of free-surface vaporization of zinc, cadmium and mercury oxides analyzed by the third-law method. *Thermochim. Acta.* 411 (2), 187–193. http://dx.doi.org/10.1016/j.tca.2003.08.024.

Liu, G.L., Cabrera, J., Allen, M., Cai, Y. 2006. Mercury characterization in a soil sample collected nearby the DOE Oak Ridge Reservation utilizing sequential extraction and thermal desorption method. *Sci. Total. Environ.* 369 (1–3), 384–392. http://dx.doi.org/10.1016/j.scitotenv.2006.07.011.

Lopez-Anton, M.A., Yuan, Y., Perry, R., Maroto-Valer, M.M. 2010. Analysis of mercury species present during coal combustion by thermal desorption. *Fuel.* 89 (3), 629–634. http://dx.doi.org/10.1016/j.fuel.2009.08.034.

López-Delgado, A., López, F.A., Alguacil, F.J., Padilla, I., Guerrero, A. 2012a. A microencapsulation process of liquid mercury by sulfur polymer stabilization/solidification technology. Part I: Characterization of Materials. *Rev. Metal.* 48 (1), 45–57. http://dx.doi.org/ 10.3989/revmetalm.1133.

López-Delgado, A., Guerrero, A., López, F.A., Pérez, C., Alguacil, F.J. 2012b. A microencapsulation process of liquid mercury by sulfur polymer stabilization/solidification technology. Part II: Durability of Materials. *Rev. Metal.* 48 (1), 58–66. http://dx.doi.org/10.3989/revmetalm.1137.

Loveday, J., Beatty, H.J., Norris, J.M. 1972. Comparison of current chemical methods for evaluating irrigation soils. *CSIRO Australia, Division of Soils, Technical Paper* 14.

MAPA. 1994. Métodos oficiales de Análisis: Tomo III. (Ministerio de Agricultura, Pesca y Alimentación). Madrid (Spain): Secretaría General Técnica.

Millan, R., Gamarra, R., Schmid, T., Sierra, M.J., Quejido, A.J., Sanchez, D.M., Cardona, A.I., Fernandez, A., Vera, R. 2006. Mercury content in vegetation and soils of the Almaden mining area (Spain). *Sci. Total. Environ.* 368 (1), 79–87. http://dx.doi.org/10.1016/j.scitotenv.2005.09.096.

Millan, R., Schmid, T., Sierra, M.J., Carrasco-Gil, S., Villadoniga, M., Rico, C., Ledesma, D.M.S., Puente, F.J.D. 2011. Spatial variation of biological and pedological properties in an area affected by a metallurgical mercury plant: Almadenejos (Spain). *Appl. Geochem.* 26 (2), 174–181. http://dx.doi.org/10.1016/j.apgeochem.2010.11.016.

Oliveira, L.C., Botero, W.G., Santos, F.A., Jr., É.S., Rocha, J.C., Santos, A. 2012. Influence of Seasonality on the Interaction of Mercury with Aquatic Humic Substances Extracted from the Middle Negro River Basin (Amazon). *J. Braz. Chem. Soc.* 23 (9), 1711–1718. http://dx.doi.org/S0103-505320120050000034.

Ozaki, M., Uddin, M.A., Sasaoka, E., Wu, S.J. 2008. Temperature programmed decomposition desorption of the mercury species over spent iron-based sorbents for mercury removal from coal derived fuel gas. *Fuel.* 87 (17–18), 3610-3615. http://dx.doi.org/10.1016/j.fuel.2008.06.011

Ozawa, T., 1965. A new method of analizing thermogravimetric data. *Bull. Chem. Soc. Jpn.* 38 (11), 1881–1884. http://dx.doi.org/10.1246/bcsj.38.1881.

Page, A.L., Miller, R.H., Heeney, D.R. 1987. Methods of soil analysis. Part 2. Chemical and microbiological properties. Ed. American Society of Agronomy, Soil Science Society of America. Madison, Wisconsin (USA).

Paruchuri, Y., Siuniak, A., Johnson, N., Levin, E., Mitchell, K., Goodrich, J.M., Renne, E.P., Basu, N. 2010. Occupational and environmental mercury exposure among small-scale gold miners in the Talensi-Nabdam District of Ghana's Upper East region. *Sci. Total. Environ.* 408 (24), 6079–6085. http://dx.doi.org/10.1016/j.scitotenv.2010.08.022.

Plante, A.F., Fernández, J.M., Leifeld, J. 2009. Application of thermal analysis techniques in soil science. *Geoderma.* 153 (1–2), 1–10. http://dx.doi.org/10.1016/j.geoderma.2009.08.016.

Salgado, J., González, M.I., Armada, J., Paz-Andrade, M.I., Carballas, M., Carballas, T. 1995. Loss of organic matter in Atlantic forest soils due to wildfires. Calculation of the ignition temperature. *Thermochim. Acta.* 259 (1), 165–175. http://dx.doi.org/10.1016/0040-6031(95)02274-6.

Salgado, J., Mato, M.M., Vázquez-Galiñanes, A., Paz-Andrade, M.I., Carballas, T. 2004. Comparison of two calorimetric methods to determine the loss of organic matter in Galician soils (NW Spain) due to forest wildfires. *Thermochim. Acta.* 410 (1–2), 141–148. http://dx.doi.org/10.1016/S0040-6031(03)00400-3.

Skyllberg, U., Bloom, P.R., Qian, J., Lin, C.M., Bleam, W.F. 2006. Complexation of mercury(II) in soil organic matter: EXAFS evidence for linear two-coordination with reduced sulfur groups. *Environ. Sci. Technol.* 40 (13), 4174–4180. http://dx.doi.org/10.1021/es0600577.

Stein, E.D., Cohen, Y., Winer, A.M. 1996. Environmental distribution and transformation of mercury compounds. *Crit. Rev. Environ. Sci. Technol.* 26 (1), 1–43.

USEPA. 1996. Method 3052. Washington D.C.: EPA Office of Solid Waste.

USEPA. 2008. Land disposal restrictions: Regulations for mercury-containing non waste waters. R 40CFR Part 273.

Vyazovkin, S. 2001. Modification of the integral isoconversional method to account for variation in the activation energy. *J. Comput. Chem.* 22 (2), 178–183. http://dx.doi.org/10.1002/1096-987x(20010130)22:2<178::aid-jcc5>3.0.co;2-#.

Wang, J.X., Feng, X.B., Anderson, C.W.N., Xing, Y., Shang, L.H. 2012. Remediation of mercury contaminated sites - A review. *J. Hazard. Mater.* 221, 1–18. http://dx.doi.org/10.1016/j.jhazmat.2012.04.035.

Windmoller, C.C., Wilken, R.D., Jardim, W.D. 1996. Mercury speciation in contaminated soils by thermal release analysis. *Water. Air. Soil. Poll.* 89 (3–4), 399–416. http://dx.doi.org/10.1007/bf00171644.